

**Original Article**

DOI 10.1007/s12206-022-0135-5

**Keywords:**

- BPNN training algorithm
- Signal processing
- SBLMD
- Stability
- Chatter index

**Correspondence to:**Rohit Mishra  
rohitmishra2288@gmail.com**Citation:**Mishra, R., Singh, B. (2022). Prediction of milling chatter using SBLMD-ANN. *Journal of Mechanical Science and Technology* 36 (2) (2022) 877~882.  
<http://doi.org/10.1007/s12206-022-0135-5>

Received March 15th, 2021

Revised August 7th, 2021

Accepted October 8th, 2021

† Recommended by Editor  
Hyung Wook Park

# Prediction of milling chatter using SBLMD-ANN

**Rohit Mishra and Bhagat Singh**

Jaypee University of Engineering and Technology, Guna (M.P.), India

**Abstract** In the present study, acquired audio signal in milling operation is processed in order to extract tool chatter features. Further, six artificial neural network (ANN) training algorithms viz. Resilient propagation (RP), conjugate gradient based (CGP and SCG), quasi-Newton based (BFGS and OSS) and Levenberg-Marquardt algorithm (LM) are used to train the data set. Among these, the most suitable one has been selected and further invoked to develop prediction model of chatter severity in terms of chatter indicator (CI). Finally, developed prediction model has been critically explored to analyze milling stability conditions.

## 1. Introduction

Regenerative chatter is a very common and complex phenomenon often encountered in milling process. Major limitations of regenerative vibrations are low yield, poor surface finish and tool damage. Chatter is highly influence by the machining parameters and also their interaction effects. So, it is pretty important that a technique should be adapted for selecting the suitable range of machining parameters [1]. Analytical approaches has been used by the researchers to explore chatter [2, 3]. But, due to very intricate cutting situation, diagnostic is not easy.

To overcome such hindrance, researches have proposed and used various novel self adaptive techniques in recent years such as empirical mode decomposition (EMD) and ensemble empirical mode decomposition (EEMD), local mean decomposition (LMD) and variational mode decomposition (VMD). However, all these self adaptive signal processing techniques have their own limitations. In EMD and EEMD, mode aliasing, end effect and overshoot-undershoot is the main problem [4, 5]. In LMD, one of the troublesome problems is the calculation of efficient and accurate local mean and envelope estimate functions [6]. In VMD, it is the requirement to provide the mode number in its early stage. If the provided mode number is wrong, then VMD will result in the loss of important modes [7]. Therefore, to remove these weaknesses and to improve its efficiency and accuracy, recently an improved spline based - LMD (SBLMD) method came into existence [8]. From the previous research, it has been found that machining performance and tool life can be improved by altering the properties of cutting tool [9-11].

After signal processing and feature extraction, it is quite essential to develop a chatter severity model. Artificial neural network (ANN) has been used by researchers for the assessment of cutting forces, surface roughness and tool wear during machining operations [12]. Main concern in ANN modeling is to select the training function and optimized number of neurons in the hidden layer. In the present work, an attempt has been made to overcome aforementioned issues.

The rest of paper is organized as follows: Sec. 2 enumerates proposed signal processing technique. In Sec. 3, experimentations details are presented. ANN modeling of chatter severity and details related to selection of optimized neurons in hidden layer and training function is presented in Sec. 4. Result and discussion is presented in Sec. 5. At last, the conclusions drawn are summed up in Sec. 6.

## 2. Spline based local mean decomposition

In this signal processing technique, the cubic spline substitutes the moving average in the

Table 1. Experimental settings.

Parameters	Level 1	Level 2	Level 3
Spindle speed (N, rpm)	1000	2000	3000
Feed rate (F, mm/min)	50	75	100
Axial depth of cut (D, mm)	1	1.5	2

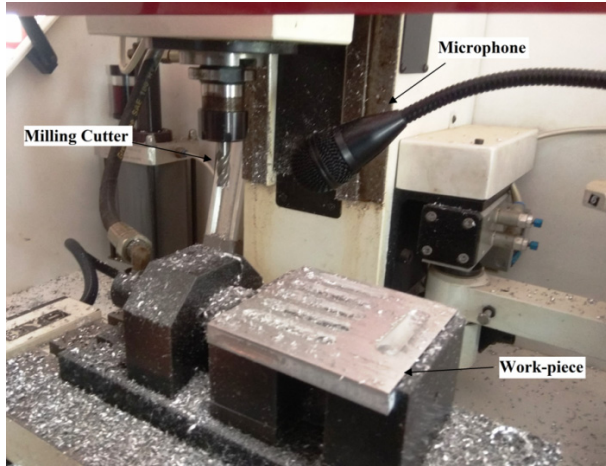


Fig. 1. Set up for signal acquisition during experiments.

traditional LMD. Following steps are used to achieve the PF's.

1) To begin, locate all of the signal's local extremes. Then one cubic spline is used for upper maxima and another one for connecting all local minima. This would result in the formation of the upper and lower layer, denoted by  $P_u(t)$  and  $P_l(t)$ .

2) The terms in Eq. (1) can be used to calculate the local mean and envelope functions, denoted by  $m_{11}(t)$  and  $a_{11}(t)$ .

$$m_{11}(t) = \frac{P_u(t) + P_l(t)}{2} \quad a_{11}(t) = \frac{|P_u(t) - P_l(t)|}{2} \quad (1)$$

3) The final steps will be the same as in the traditional LMD algorithm.

### 3. Experimental setup

For performing the end milling experiments, four fluted HSS milling cutter and Al 6061-T6 series (ASTM B-308 standard) as a workpiece has been selected. Fig. 1 shows the Photograph of the experimental set-up. Microphone (model no: AHUJA AGN-480) having 600  $\Omega$  impedance and 2 mV/Pa sensitivity, has been used for acquiring the generated sound signals (real working signal) during machining. Total 27 experiments have been performed with full factorial combinations of the input parameters, as presented in Table 1.

#### 3.1 Processing by LMD

PF's of the selected signal are displayed in Fig. 2, after they have been processed using LMD.

After disintegrating, there are total of 8 PF's. The coefficient

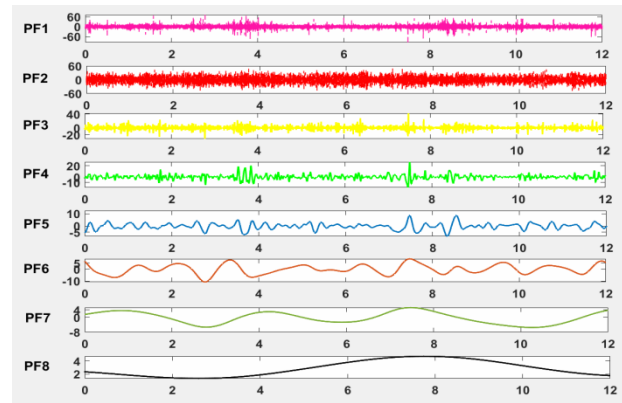


Fig. 2. PF's extracted using LMD.

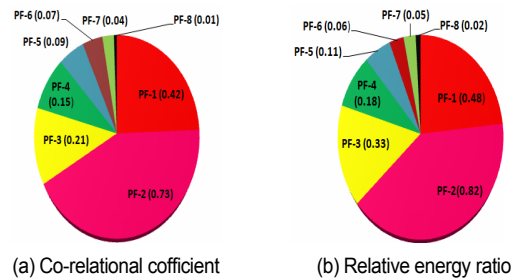


Fig. 3. (a) CC; (b) RER.

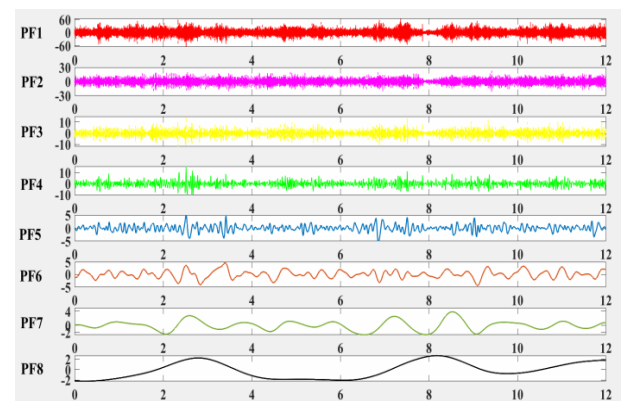


Fig. 4. PF's extracted using SBLMD.

of correlation (CC) and energy ratio (RER) are used and compared for obtained PF's. These indicators are selected for extracting the useful data and discarding the noise content. It is clear from Fig. 3 that first three PF's are crucial since first three PF's having higher energy ratio as well as higher co-relation coefficient. But after reconstructing the signal, it has been observed that frequency peaks are not clearly distinguishable.

#### 3.2 Processing by SBLMD

For extracting the useful and constructive details and filtering the unwanted noise data from sound signal, SB-LMD technique is applied. Signal is treated with new LMD and obtained product functions (PF's) are shown in Fig. 4.

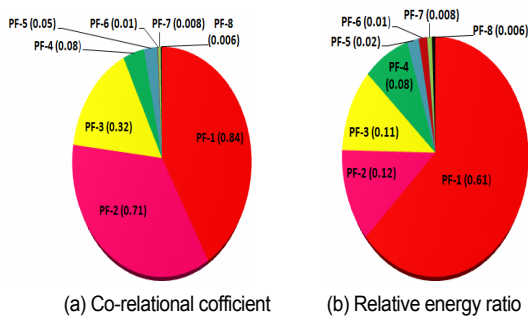


Fig. 5. CC and RER of PF's.

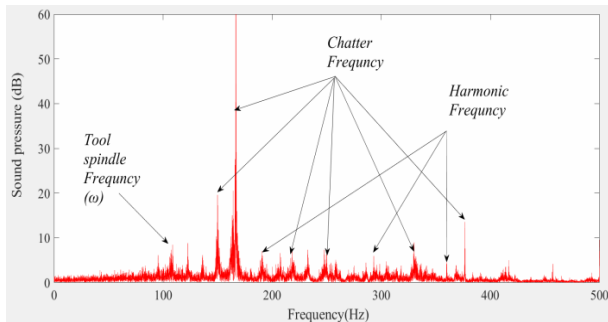


Fig. 6. FFT of SBLMD processed reconstructed signal.

It is clear from Fig. 5 that first three PFs are crucial since first three PF's having higher energy ratio as well as higher co-relation coefficient. Since first three PF's have the most critical information about a signal. These PFs are then utilized to recreate the chatter vibration signal.

SBLMD methodology is given in Fig. 6. It is clear from Fig. 6, that SBLMD is quite proficient to extract the three basic essential frequency components, i.e., spindle frequency, multiple of spindle frequency (or harmonics) and frequencies of chatter. As a result, it appears that the suggested technique is capable of perceiving chatter frequencies contained in the reconstructed signal with ease.

### 3.3 Tool chatter features extraction

Feed rate is also an important input parameter that influences the tool chatter, but this study has been previously neglected by the researchers. Main reason of the negligence is the impact of this phenomenon of tool chatter is difficult to comprehend using the stability lobe diagram (SLD). Therefore, this research gap is the impetus for the current study. In this section, the influence of feed rate is also examined. To achieve the aforementioned aim, a new expression, chatter indicator (CI), is proposed.

The coefficient of variance is used to calculate the chatter indicator. The chatter indicator was calculated for each of the 27 experimental runs and given in Table 2. To characterize the three domains of chatter seriousness, threshold limits are resolved using 3  $\sigma$  model.

Table 2. Chatter Indicator for 27 experiments.

Exp. no.	N (RPM)	F (mm/min)	D (mm)	Chatter indicator (CI)
1	1000	50	1	1.14732
2	1000	50	1.5	1.11746
3	1000	50	2	2.59148
4	1000	75	1	1.02469
5	1000	75	1.5	1.03535
6	1000	75	2	1.79562
7	1000	100	1	0.93299
8	1000	100	1.5	1.16331
9	1000	100	2	2.55056
10	2000	50	1	1.69859
11	2000	50	1.5	2.06113
12	2000	50	2	2.34157
13	2000	75	1	1.30086
14	2000	75	1.5	1.88199
15	2000	75	2	2.48315
16	2000	100	1	1.26461
17	2000	100	1.5	1.97476
18	2000	100	2	2.56952
19	3000	50	1	2.52537
20	3000	50	1.5	2.09632
21	3000	50	2	2.93336
22	3000	75	1	2.11764
23	3000	75	1.5	2.19868
24	3000	75	2	3.02613
25	3000	100	1	2.24453
26	3000	100	1.5	2.27546
27	3000	100	2	3.15835

## 4. Artificial neural network

In ANN modeling, various training functions are available and can be used for training the data. Viability of training function is problem specific. In this work, six variants of BP algorithms, named as resilient propagation (RP), conjugate gradient algorithms (CGP and SCG), quasi-Newton algorithms (BFGS and OSS) and Levenberg-Marquardt algorithm (LM), have been used to train the model in order to improve the efficiency of ANN for producing better prediction models for chatter identification. Before training the network, neuron selection plays an important role for the better prediction.

### 4.1 Selection of number of neurons in the hidden layer

In this study, number of neurons has been optimized by using mean squared error (MSE). In order to achieve the optimized neurons, data have been trained for all selected training algorithm by varying the neuron numbers from 1 to 30. Calcula-

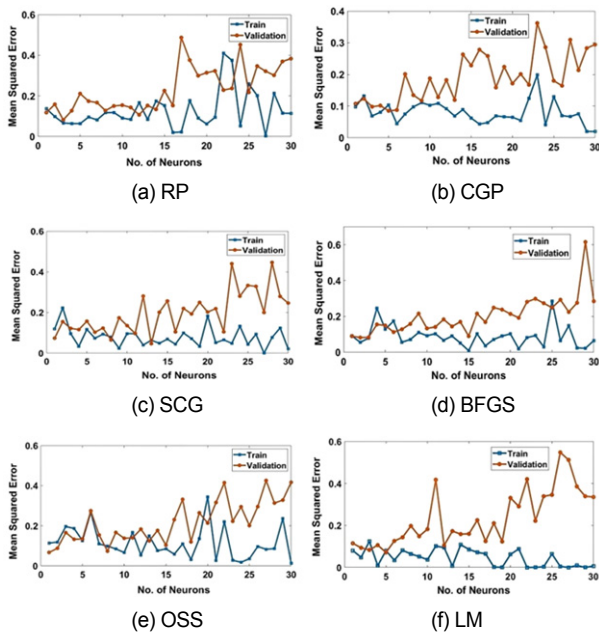


Fig. 7. Mean squared error v/s number of neurons for all six training algorithms.

lated mean squared errors (MSE) have been plotted against number of neurons as shown in Fig. 7.

From Fig. 7, it is observed that the optimum number of neurons for RP, CGP, SCG, BFGS, OSS and LM are 8, 9, 11, 5, 5 and 5 neurons, respectively. Later, these optimized neurons for hidden layer are used to train the data.

### 4.2 Selection of training algorithm

In order to select the best training algorithm for the prediction of chatter severity, neural network has been trained using all six training functions. Three input variables have been considered as input parameters for the input neurons layer. The output layer consists of only one neuron to predict chatter indicator. Optimized number of neurons has been for further analysis. In order to evaluate the prediction capability of the algorithms, absolute percentage deviation (APD) has been calculated and presented in Table 3. Later, final average absolute percentage deviation (AAPD) has been calculated for every algorithm.

Average absolute percentage deviation for RP, CGP, SCG, BFGS, OSS and LM are 7.49, 12.66, 14.72, 20.82, 13.07 and 3.11, respectively. Average absolute percentage deviation for LM algorithm is found to be least with respect to other algorithms.

### 4.3 Prediction model for Ci

For ANN modeling, LM algorithm as a training function along with TANSIG and PURELIN activation functions has been used successively between the hidden and input layer and output and hidden layer, respectively. The obtained optimal weight and bias between the respective layers is pre-

Table 3. Average absolute percentage deviation for selected algorithms.

Exp. no.	RP APD	CGP APD	SCG APD	BFG APD	OSS APD	LM APD
1	12.962	13.528	41.246	42.282	4.2201	1.0095
2	4.6841	33.652	88.418	32.204	30.901	4.4598
3	14.291	4.8296	6.4016	18.093	7.2089	2.9194
4	5.5306	4.8443	23.095	47.015	5.1139	0.1915
5	3.3997	1.7163	7.6546	44.276	20.520	3.8268
6	6.8097	32.449	1.7307	0.2304	14.567	4.6853
7	19.159	2.4973	10.009	59.768	24.453	0.1175
8	0.4179	16.979	9.0080	31.307	42.838	11.313
9	20.396	13.973	29.179	36.628	18.784	12.805
10	3.0821	10.876	24.563	0.7131	6.1681	5.2323
11	7.1860	20.046	1.8322	3.2502	0.5366	4.8134
12	5.7449	15.023	30.812	18.358	12.343	1.4798
13	6.8547	11.929	2.8288	19.380	40.877	2.0317
14	8.8728	5.1531	11.777	10.231	10.850	5.6192
15	6.9963	2.0393	15.718	8.8074	5.0273	0.6175
16	7.6375	20.443	12.014	17.449	1.9233	4.6750
17	5.0275	3.8775	6.1639	20.555	29.536	1.2614
18	1.5298	7.2358	11.005	7.5603	14.154	2.1081
19	10.091	24.109	41.570	14.784	13.612	1.1488
20	7.6863	13.473	0.7990	32.082	6.8720	0.0203
21	12.497	19.842	7.1071	3.0449	4.4196	0.8546
22	0.2427	1.8717	2.7244	21.686	11.811	2.6473
23	3.6049	9.5566	3.3690	16.749	8.2634	2.1756
24	9.1277	2.6816	2.9496	6.0303	2.4367	3.9128
25	4.8555	9.4816	0.3437	32.665	6.5686	3.6737
26	8.0697	30.405	4.1571	6.2849	4.8565	0.2670
27	5.5993	9.4035	1.1296	10.676	4.2215	0.2727
AAPD	7.4947	12.663	14.726	20.819	13.077	3.1163

sented in Tables 4 and 5.

### 4.4 Development of mathematical expression

Mathematical expression for hidden layer is expressed as:

$$\begin{aligned}
 z_1^2 &= \theta_{11}^1 \times a_1^1 + \theta_{12}^1 \times a_2^1 + \theta_{13}^1 \times a_3^1 + \theta_{10}^1 \\
 z_2^2 &= \theta_{21}^1 \times a_1^1 + \theta_{22}^1 \times a_2^1 + \theta_{23}^1 \times a_3^1 + \theta_{20}^1 \\
 z_3^2 &= \theta_{31}^1 \times a_1^1 + \theta_{32}^1 \times a_2^1 + \theta_{33}^1 \times a_3^1 + \theta_{30}^1, \\
 z_4^2 &= \theta_{41}^1 \times a_1^1 + \theta_{42}^1 \times a_2^1 + \theta_{43}^1 \times a_3^1 + \theta_{40}^1 \\
 z_5^2 &= \theta_{51}^1 \times a_1^1 + \theta_{52}^1 \times a_2^1 + \theta_{53}^1 \times a_3^1 + \theta_{50}^1
 \end{aligned}$$

where;  $\theta$  is the weight,  $\theta$  superscript represents the connection between the layers (input to hidden layer), first number in  $\theta$  subscript is representing the position of neuron in the second layer. Second number in  $\theta$  subscript is the position of neuron in the first layer. To get the value of neurons in the hidden layer,  $z$  values need to be fed in to the activation function (TANSIG).

Table 4. Weight to hidden layer from input layer.

Neurons	$a_1^1(ss_n)$	$a_2^1(F_n)$	$a_3^1(D_n)$	$bias^1$
$a_1^2$	0.96957	-3.1665	0.53242	-2.9347
$a_2^2$	-1.6207	0.14413	3.243	-1.0427
$a_3^2$	-2.6834	0.041645	2.333	-0.80378
$a_4^2$	1.3065	0.81295	1.1194	0.85065
$a_5^2$	0.93809	1.9373	0.96782	1.111

Table 5. Weight to output layer from hidden layer.

Neuron	$a_1^2$	$a_2^2$	$a_3^2$	$a_4^2$	$a_5^2$	$bias^2$
$a_1^3(CI_n)$	-0.847	1.802	-1.72	2.0199	-1.860	-0.732

Now, neurons in the hidden layer are calculated using the expressions;

$$a_1^2 = \frac{2}{1 + e^{-2 \times a_1^1}} - 1; a_2^2 = \frac{2}{1 + e^{-2 \times a_2^1}} - 1;$$

$$a_3^2 = \frac{2}{1 + e^{-2 \times a_3^1}} - 1; a_4^2 = \frac{2}{1 + e^{-2 \times a_4^1}} - 1;$$

$$a_5^2 = \frac{2}{1 + e^{-2 \times a_5^1}} - 1.$$

Mathematical expression for output layer is expressed as;

$$z_1^3 = \theta_{11}^2 \times a_1^2 + \theta_{12}^2 \times a_2^2 + \theta_{13}^2 \times a_3^2 + \theta_{14}^2 \times a_4^2 + \theta_{15}^2 \times a_5^2 + \theta_{10}^2.$$

To get the value of neuron at the output layer, PURELIN function is used. So, neuron value in the output is determined using the following expression

$$a_1^3(CI_n) = z_1^3.$$

## 5. Result and discussion


### 5.1 Effect of individual parameters on CI

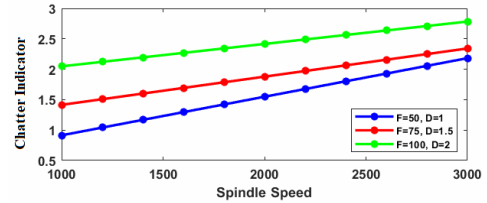
Effect of individual input parameters on CI has been shown in Fig. 8. On analyzing Fig. 8(a), it can be interpreted that spindle speed increment results in enhanced CI. It is observed that the percentage change in CI is 81.91 %, 49.35 % and 30.47 %, respectively. Percentage change in blue line which is drawn at low feed and depth of cut is higher as compared to other lines. Thus, it can be concluded that the relative effect of spindle speed is dominating at lower values of feed and axial depth of cut. From Fig. 8(b), it can be inferred that CI is not much affected by the variation in feed rate. However, percentage change in CI w.r.t. feed rate at low spindle speed and axial

Table 6. Stability range.

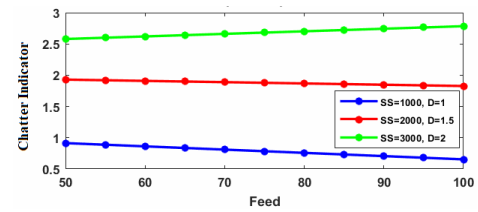
	D (mm)	F (m/min)	N (rpm)
Stability range	1.6-1.78	81-100	2380-2900

Table 7. Experimental validation.

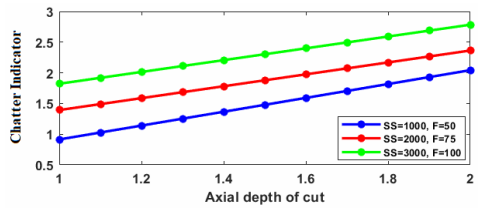
Exp. No.	D	N	F	CI	Surface view
1	1.7	2400	90	1.14	



(a)



(b)



(c)

Fig. 8. Effect of milling parameters on CI.

depth of cut is higher as compared to the rest two states. By observing Fig. 8(c), it can be deduced that CI increases with the increase in axial depth of cut. The net differences in the value of CI for blue, red and green lines are 1.129, 0.9705 and 0.962, respectively. Thus, on comparing Figs. 8(a)-(c), it can be inferred that the effect of SS and D is more pronounced.

### 5.2 Safe milling zone

After analyzing the severity of individual parameters on chatter severity, range of parameters pertaining to stable milling have been ascertained by extracting common range of values from Fig. 8 and are presented in Table 6.

In order to validate the obtained range, further experiment has been performed. This experiment has been performed considering the developed stable range and is presented in Table 7. Result of validation experiment shows that at this mill-

ing range CI value is below the threshold stability value. Moreover, surface texture of the machined surface has also been presented in Table 7. On examining this surface texture it is also evident that the developed range is correct. Thus, the proposed methodology is quite suitable for ascertaining the stable milling parameters that will result in higher productivity along with better surface finish.

## 6. Conclusions

This research is focused on the identification of chatter during milling operation. A new LMD approach based on cubic spline interpolation has been used to achieve the aforementioned objective. Further, ANN has been invoked to investigate the relative influence of milling variables on CI. This modeling has been done using the various training functions (RP, CGP, SCG, BFGS, OSS and LM). Optimal neuron numbers is decided on the basis of MSE. It has been found that LM training function and 5 neurons in hidden layer is able to predict chatter with 3.11 % deviation only as compared to other training algorithms. Later mathematical expression has been developed and used to study the influence of individual milling parameter on CI. It can be inferred that the effect of SS and D is more pronounced.

## References

- [1] L. Zhu and C. Liu, Recent progress of chatter prediction, detection and suppression in milling, *Mech. Syst. Signal Process.*, 143 (2020) 106840.
- [2] Y. Altıntaş and E. Budak, Analytical prediction of stability lobes in milling, *CIRP Ann.-Manuf. Technol.*, 44 (1) (1995) 357-362.
- [3] O. Tuysuz and Y. Altıntaş, Analytical modeling of process damping in machining, *J. Manuf. Sci. Eng.*, 141 (6) (2019) 061006.
- [4] J. De Zheng, J. S. Cheng and Y. Yang, Modified EEMD algorithm and its applications, *Journal of Vibration and Shock*, 32 (21) (2013) 21-26.
- [5] S. Wan et al., Investigation on milling chatter identification at early stage with variance ratio and Hilbert-Huang transform, *International Journal of Advanced Manufacturing Technology*, 95 (9-12) (2018) 3563-3573.
- [6] L. Deng and R. Zhao, An improved spline-local mean decomposition and its application to vibration analysis of rotating machinery with rub-impact fault, *Journal of Vibroengineering*, 16 (1) (2014) 414-433.
- [7] Z. Li et al., Independence-oriented VMD to identify fault feature for wheel set bearing fault diagnosis of high speed locomotive, *Mechanical Systems and Signal Processing*, 85 (2017) 512-529.
- [8] R. Mishra and B. Singh, Stability analysis in milling process using spline based local mean decomposition (SBLMD) technique and statistical indicators, *Meas. J. Int. Meas. Confed.*, 174 (2021) 108999.
- [9] P. V. Badiger et al., Tribological behaviour of monolayer and multilayer Ti-based thin solid films deposited on alloy steel, *Materials Research Express*, 6 (2) (2018) 026419.
- [10] P. V. Badiger, V. Desai and M. R. Ramesh, Development and characterization of Ti/TiC/TiN coatings by cathodic arc evaporation technique, *Transactions of the Indian Institute of Metals*, 70 (9) (2017) 2459-2464.
- [11] P. V. Badiger et al., Effect of cutting parameters on tool wear, cutting force and surface roughness in machining of MDN431 alloy using Al and Fe coated tools, *Materials Research Express*, 6 (1) (2018) 016401.
- [12] P. V. Badiger et al., Cutting forces, surface roughness and tool wear quality assessment using ANN and PSO approach during machining of MDN431 with TiN/AlN-coated cutting tool, *Arabian Journal for Science and Engineering*, 44 (9) (2019) 7465-7477.



**Rohit Mishra** is a Post Graduate of Mechanical Engineering from Indian Institute of Technology, Roorkee, India. His research interests include stability analysis, tool condition monitoring and signal processing.